International Journal of Pharmaceutics 365 (2009) 100–108

Contents lists available at ScienceDirect

International Journal of Pharmaceutics

journal homepage: www.elsevier.com/locate/ijpharm

Alginate–magnesium aluminum silicate films: Importance of alginate block structures

Thaned Pongjanyakul*

Faculty of Pharmaceutical Sciences, Khon Kaen University, Khon Kaen 40002, Thailand

ARTICLE INFO

Article history:
Received 11 June 2008
Received in revised form 17 August 2008
Accepted 20 August 2008
Available online 27 August 2008

Keywords:
Sodium alginate
Magnesium aluminum silicate
Block structure
Composite film
Diffusion coefficient

ABSTRACT

Sodium alginate–magnesium aluminum silicate (SA–MAS) composite dispersions were prepared and characterized for the flow behavior and morphology of their dispersed phase before casting. The high G block and high M block SA (GSA and MSA, respectively) were used. The physicochemical properties and permeabilities of the films were investigated using non-electrolyte and amine compounds in an acidic medium. The results showed that incorporation of MAS into the GSA and MSA dispersions gave identical flow behaviors and morphologies of MAS flocculates. FTIR spectroscopy revealed that the GSA and MSA presented similar molecular interactions with MAS in the films. However, the crystallinity of the GSA–MAS films was possibly higher than that of the MSA–MAS films. This indicated a higher density of matrix structure formed between GSA and MAS, resulting in lower water uptake in an acidic medium. Consequently, the permeability of the GSA–MAS films was lower than that of the MSA–MAS films. The diffusion and partition coefficients were directly related to the molecular weight of the non-electrolyte and amine compounds. This study suggested that transport of non-electrolyte compounds was predominantly controlled by diffusion in aqueous-filled microchannels, whereas both partition via adsorption onto MAS and diffusion in microchannels occurred concurrently for amine compounds.

1. Introduction

Magnesium aluminum silicate (MAS) is a mixture of natural smectite clays, particularly montmorillonites and saponites (Kibbe, 2000). It has a layer structure that is composed of tetrahedrally coordinated silica atoms fused into an edge-shared octahedral plane of either aluminum hydroxide or magnesium hydroxide (Alexandre and Dubois, 2000; Kibbe, 2000). The layered structures of MAS can be separated when they are hydrated in water. Once MAS is hydrated, the weakly positively charged edges are attracted to the negatively charged faces of the colloidal layers of MAS. The face to edge attraction of these colloidal layers creates a three-dimensional colloidal structure throughout the dispersion that exhibits thixotropic properties (Zatz and Kushla, 1989). Thus, MAS has been widely used in pharmaceutical development as a suspending and stabilizing agent (Kibbe, 2000). Moreover, the positively charged edges on the layers of MAS could interact with anionic polymers, such as xanthan gum (Ciullo, 1981), carbomer (Ciullo and Braun, 1991) and sodium alginate (SA) (Pongjanyakul et al., 2005a), resulting in viscosity synergism and increases in the thixothopic properties of polymeric dispersions.

SA is a sodium salt of alginic acid, a naturally occurring nontoxic polysaccharide found in brown algae. Alginate has been widely used as a food and pharmaceutical additive, a tablet disintegrant and gelling agent. It contains two uronic acids, α-L-guluronic (G) and β-D-mannuronic acids (M) (Fig. 1), and is composed of homopolymeric blocks and blocks with alternating sequences (Draget, 2000). Generally, insoluble gel formation has been demonstrated to result from specific interactions between calcium ions and blocks of G residues in SA (Kohn, 1975). A cross-linked film between SA and divalent ions has also been prepared and some of its physical properties have been investigated, such as water vapor transmission (Remuñán-López and Bodmeier, 1997) and drug permeability (Julian et al., 1988; Aslani and Kennedy, 1996; Remuñán-López and Bodmeier, 1997; Sriamornsak and Kennedy, 2008). Recently, Russo et al. (2007) reported that cross-linked SA films prepared using various M/G ratios of SA caused a change in thermal behavior and water vapor permeability.

According to interaction between MAS and SA, composite films of both materials have been prepared, and it has been proven that this composite film is a phase-separated microcomposite. Physicochemical properties and water vapor and drug permeability of the composite films were investigated (Pongjanyakul et al., 2005b).

* Tel.: +66 43 362092; fax: +66 43 362092.
E-mail address: thaned@kku.ac.th.

0378-5173/$ – see front matter © 2008 Elsevier B.V. All rights reserved.
doi:10.1016/j.ijpharm.2008.08.025

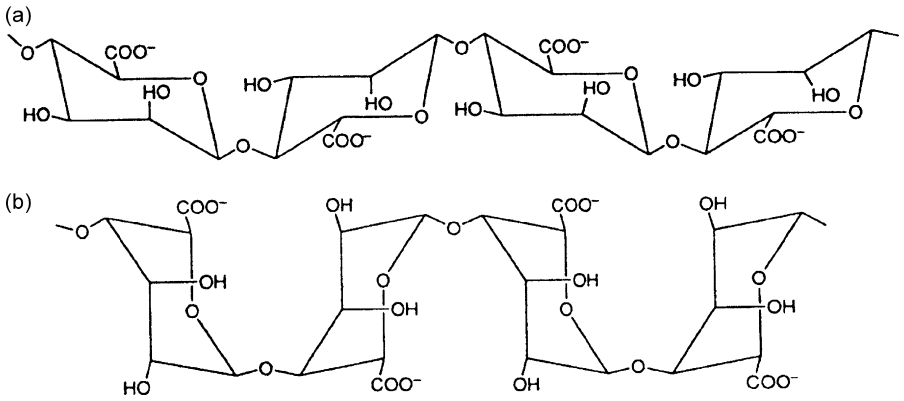

Fig. 1. Molecular structures of β-D-mannuronic acids (a) and α-L-guluronic (b) of sodium alginate.

Moreover, the SA–MAS composite dispersions were employed as a coating material for tablets, and the coated films could modulate drug release, especially in an acidic medium, because SA was converted to alginic acid, and then in situ insoluble composite films were formed for controlling drug release. However, the SA used in the previous study (Pongjanyakul et al., 2005b) was a high M block grade, in which the M/G ratio was 1.6 (Lemoine et al., 1998). Due to the different properties of M and G block residues, the interaction between MAS and SA with various M/G ratios may occur differently, which may influence the physicochemical and permeability characteristics of the SA–MAS composite films. Moreover, it is possible to use the composite films with other drugs; therefore, the permeability test needs to be investigated using many drugs.

In the present study, the composite dispersions were prepared at the weight ratio of 1:1 of MAS and SA, with high G block (GSA) or high M block (MSA) contents. The flow behavior and morphology of the dispersed phases of the composite dispersions were initially characterized before casting onto a plastic mold and drying to obtain the composite films. Then, interactions of MAS were investigated with different block structures of SA in the film by FTIR spectroscopy. The physicochemical properties of the composite films, such as thermal behavior, solid-state crystallinity, water uptake, and water vapor permeability, were investigated. Additionally, the permeability of the composite films in an acidic medium was characterized using non-electrolyte and amine compounds for elucidating the relationship between molecular weight (MW) of the compounds and permeation parameters. The relationships obtained can be applied to predict drug release behavior from coated tablets in an acidic medium.

2. Materials and methods

2.1. Materials

High G block sodium alginate (GSA, ratio of M/G = 0.59) and high M block sodium alginate (MSA, ratio of M/G = 1.50) were obtained from ISP Thailand Ltd. (Bangkok, Thailand). MAS (Veegum®HV) was obtained from R.T. Vanderbilt Company, Inc. (Norwalk, CT, USA). Nicotine (NCT), methylparaben (MP), propylparaben (PP), and butylparaben (BP) were obtained from Fluka (Buchs, Switzerland). Propranolol HCl (PPN), dextromethorphan HBr (DTM), and acetaminophen (ACT) were purchased from Praporn Darsut Ltd. (Bangkok, Thailand). Diphenhydramine HCl (DPH) was purchased from and Srichand United Dispensary Company, Ltd. (Bangkok, Thailand). Other reagents used were of analytical grade and used as received.

2.2. Preparation of dispersions

SA (2 g) was dispersed in distilled water with agitation to obtain homogeneous gels. MAS (2 g) was pre-hydrated with hot water for 15 min and then added into the SA gel. The composite dispersions were adjusted to a final volume of 200 ml with distilled water. The dispersions were mixed with a homogenizer for 5 min and at room temperature during hydration and before use. The SA dispersions without MAS were prepared using the method as described above.

2.3. Preparation of films

SA and SA–MAS composite films were prepared using the casting/solvent evaporation technique that has been previously reported (Remuñán-López and Bodmeier, 1997). A 200 ml sample of the SA or SA–MAS dispersion was poured onto a plastic plate (15 cm × 20 cm) and allowed to evaporate at 50 °C. The films were peeled off and stored in a desiccator (40 ± 2% RH).

2.4. Characterization of composite dispersions

The microscopic morphology of the MAS particles and SA–MAS flocculates in dispersion were investigated using an inverted microscope (Eclipse TS100, Nikon, Japan) and examined with a digital camera (Coolpix 4500, Nikon, Japan). The rheological properties of the dispersions were studied using a Brookfield digital rheometer (Model DV-III, Brookfield Engineering Laboratories, Inc., Middleboro, MA, USA) and the condition used was described in the previous study (Pongjanyakul et al., 2005a). The area of the hysteresis loop of the rheogram was computed from the difference between the area under the up-curve and the down-curve using the trapezoidal rule. Moreover, other rheological parameters of the dispersions were calculated using the following equations (Martin, 1993):

$$F^N = \eta G \quad (1)$$

$$\log G = N \log F - \log \eta \quad (2)$$

where G, F, N and η are shear rate, shear stress, exponential constant that defines the type of flow, and viscosity coefficient, respectively.

2.5. Characterization of composite films

2.5.1. Thickness of films

The thickness of the dry and wet films was measured in 12 places using a microprocessor coating thickness gauge (Minitest 600B, ElektroPhysik, Germany). The dry films (4 cm × 4 cm) were cut and placed on a control plate. The probe, which was connected

Table 1
Rheological properties of SA and SA–MAS dispersions

Dispersion	N	Viscosity coefficient ([dyne cm^{-2}]^N s)	Area of hysteresis loop (dyne cm^{-2} s^{-1})
GSA	0.88 ± 0.01	1.04 ± 0.08	2.56 ± 1.95
MSA	0.82 ± 0.02	0.78 ± 0.04	3.29 ± 0.73
GSA–MAS	1.33 ± 0.03	5.38 ± 0.55	7.60 ± 0.72
MSA–MAS	1.37 ± 0.07	5.63 ± 1.26	9.28 ± 1.03

Data are the mean ± S.D., $n = 3$.

to the measurement gauge and calibrated using a standard film, gently moved downward to touch the film, and the thickness of film was then measured. The films were subsequently placed in a small beaker containing 0.1 M HCl, which was shaken occasionally in a water bath at 37.0 ± 0.5 °C for 30 min. The samples were taken and blotted to remove excess water. The thickness of the wet films was immediately determined following the procedure mentioned above.

2.5.2. DSC, PXRD and FTIR spectroscopy

DSC curves of samples were recorded using a differential scanning calorimeter (DSC822, Mettler Toledo, Switzerland). Powder X-ray diffraction (PXRD) measurements of samples were performed on a powder X-ray diffractometer (Philips PW3710 mpd control, The Netherlands). FTIR spectra of samples were recorded with an FTIR spectrophotometer (Spectrum One, Perkin Elmer, Norwalk, CT) using the KBr disc method. The methods and conditions used for measurement were similar to those in the previous study (Pongjanyakul and Puttipipatkhachorn, 2007).

2.5.3. Water uptake and erosion of films

Water uptake and erosion of the films were carried out using the gravimetric method. Films measuring 1.5 cm × 1.5 cm were weighed (W_0) and then soaked in 0.1 M HCl and shaken occasionally at 37.0 ± 0.5 °C. After a predetermined time interval, each film was withdrawn, blotted to remove excess water, immediately weighed (W_t), and then dried in a hot air oven at 50 °C to a constant weight (W_d). The percent water uptake and percent erosion can be calculated from the following equation (Tuovinen et al., 2003):

$$\text{water uptake}\,(\%) = \left(\frac{W_t - W_d}{W_d}\right) \times 100 \quad (3)$$

$$\text{erosion}\,(\%) = \left(\frac{W_0 - W_d}{W_0}\right) \times 100 \quad (4)$$

where W_0, W_t and W_d are the original, wet and dry weights of the films, respectively.

2.5.4. Water vapor permeability of film

Water vapor permeation (WVP) across the films was studied following the method that was described in the previous study (Pongjanyakul and Puttipipatkhachorn, 2007). The WVP rate was obtained from the slope of relationship of the amount of water permeated and time. The WVP coefficient of the films was calculated using the following equation (Porter and Ridgway, 1982; Limmatvapirat et al., 2004):

$$\text{WVP coefficient} = \frac{Mh}{A\ \Delta P_v} \quad (5)$$

where M is the WVP rate, h is the mean thickness of the film, A is the area of the exposed film, and ΔP_v is the vapor pressure difference.

2.5.5. Permeability studies of films

Permeability of the films was studied using two groups of compounds. The first group consisted of the non-electrolyte compounds, such as ACT (MW = 151.2), MP (MW = 152.2), PP (MW = 180.2), and BP (MW = 194.23). The second group included the amine compounds, such as NCT (MW = 162.2), DPH (MW in free base form = 255.4), PPN (MW in free base form = 259.3), and DTM (MW in free base form = 271.4). The permeation of compounds through the films was studied using a horizontal side-bi-side diffusion cell (Crown Glass Co., Inc., Somerville, NJ) at 37.0 ± 0.5 °C. The films that had been hydrated in 0.1 M HCl for 30 min were clamped between donor and receptor compartments in a 3 ml volume, and the diffusional area was 0.66 cm^2. The solutions of permeants (4 mg/ml) or suspensions of parabens in 0.1 M HCl were placed in the donor compartment, while the receptor compartment was 3 ml of 0.1 M HCl. Both compartments were stirred continuously throughout the tests. At appropriate time intervals, 2.5 ml aliquots of the receptor medium were withdrawn and immediately replaced with fresh medium. The amount of compound permeated was analyzed using UV–vis spectrophotometry (Shimadzu UV1201, Japan) at the maximum absorption wavelength of each compound.

The paraben suspensions were prepared by adding an excess amount of paraben into a test tube containing 10 ml of 0.1 M HCl. Then, the tubes were shaken at 37 °C for 3 days until a saturated solution of parabens was obtained. The concentration of parabens in the supernatant was analyzed using UV–vis spectrophotometry at a wavelength of 256 nm (Shimadzu UV1201, Japan). The suspensions of parabens (3 ml) were used as the donor compartments and the saturated concentrations of parabens were also used to calculate the permeability coefficients of the films.

Drug permeation through a polymeric film was determined under steady state conditions by mean of Fick's first law, which can be expressed as (Martin, 1993):

$$\frac{dQ}{Adt} = PC_0 \quad (6)$$

where dQ/Adt is the permeation flux, which is the slope value calculated using linear regression analysis of the linear relationship between the amount of permeant and time, A is the surface area of the film in which the diffusion is taking place, C_0 is the concentration of permeant in the donor compartment which is assumed a constant throughout the test, and P is the permeability coefficient. The apparent diffusion coefficient (D) can be estimated using the following equation:

$$t_L = \frac{h^2}{6D} \quad (7)$$

where t_L is the lag time, which is obtained from the x-intercept of the permeation profiles, and h is the mean thickness of the films. Thus, the apparent partition coefficient (K) is obtained as follows:

$$K = \frac{Ph}{D} \quad (8)$$

3. Results and discussion

3.1. Interaction of SA with MAS in dispersions and films

The interaction between different block structures of SA and MAS in dispersions was studied by determining the change of flow behavior and microscopic morphology of MAS. The microscopic

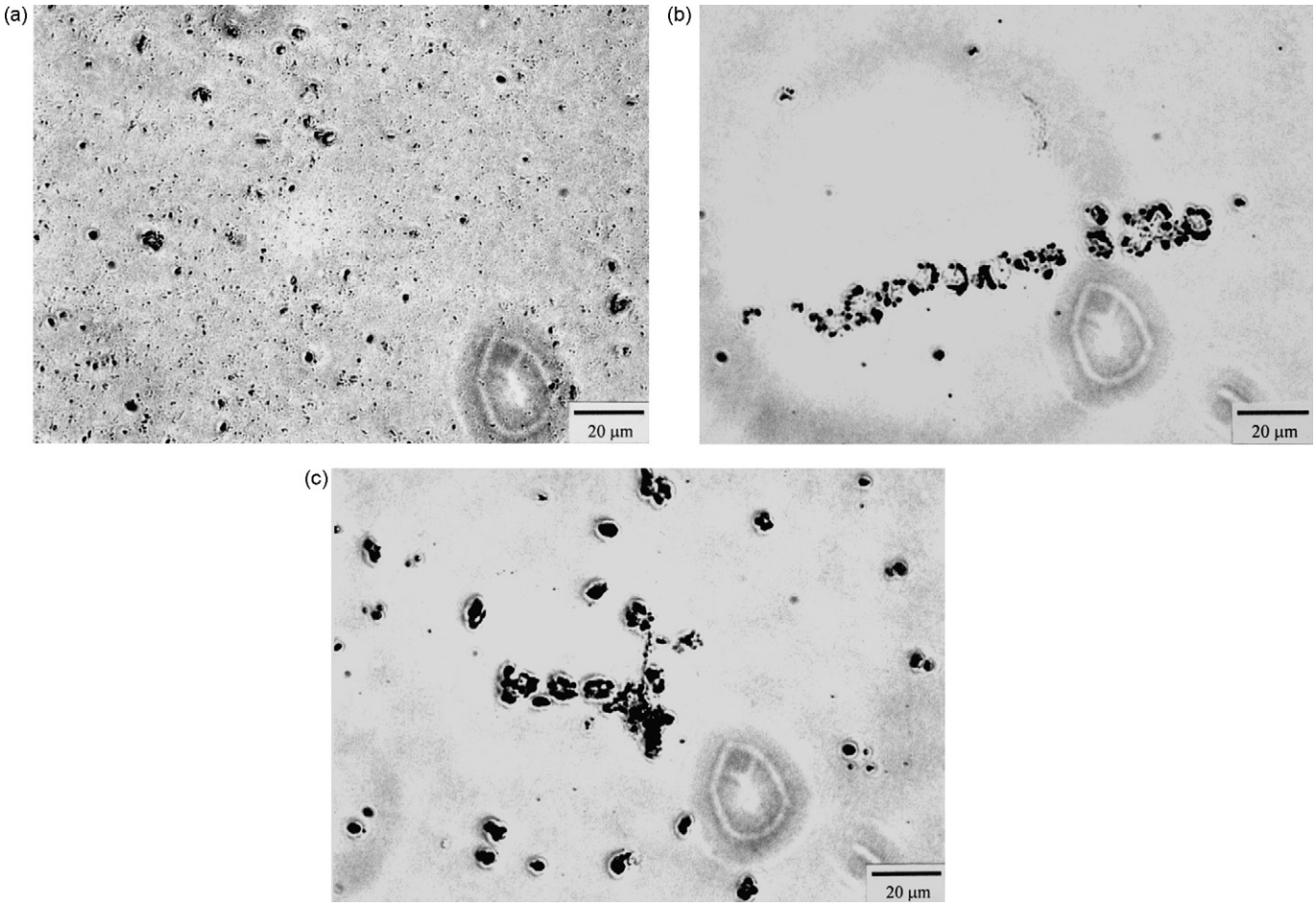

Fig. 2. Microscopic morphology of MAS in 1% MAS (a), GSA–MAS (b), and MSA–MAS (c) dispersions.

morphology of 1% MAS dispersion showed separated particles of hydrated MAS (Fig. 2a). A unique arrangement of some MAS particles was found in the GSA–MAS and MSA–MAS dispersions (Fig. 2b and c, respectively). This indicated the presence of an interaction of SA with MAS in the dispersions, resulting in a flocculation. The rheological parameters of the SA and SA–MAS dispersions are presented in Table 1. The GSA and MSA dispersions showed Newtonian flow with an N value that defined a type of flow closed to unity. Incorporating MAS into the GSA and MSA dispersions caused higher N values and viscosity coefficients, indicating a shift from a Newtonian to a pseudoplastic flow and a viscosity synergism (Martin, 1993). Moreover, the area of the hysteresis loop between the up-curve and down-curve of the flow curve also increased with MAS. This suggested the presence of a thixotropic property of the composite dispersion.

The interaction between GSA or MSA and MAS in the films was investigated using FTIR spectroscopy. Fig. 3a shows the peaks of MAS, such as the hydroxyl stretching of SiOH (3628 cm^{-1}), hydroxyl stretching of hydrogen bonded water (3461 cm^{-1}), hydroxyl bending (1642 cm^{-1}), and the stretching of Si–O–Si (1015 cm^{-1}) (Katti et al., 2006). FTIR spectra of GSA and MSA films showed similar stretching peaks of OH, COO^- (symmetric), and COO^- (asymmetric) at around 3435, 1610, and 1416 cm^{-1}, respectively (Fig. 3b and c). The obvious difference between the GSA and MSA spectra is the stretching peak of C–O–C around 1033–1125 cm^{-1}. Incorporation of MAS caused a shift to a higher wavenumber and decreased the intensity of both COO^- stretching peaks of SA (Fig. 3d and e), suggesting that the negative charge of the carboxyl groups had an electrostatic interaction with the positive charged sites in the edges of MAS. Moreover, the OH stretching

Table 2
Thickness and permeability of SA and SA–MAS films

Film	Dry thickness[a] (μm)	Wet thickness[a] (μm)	Thickness increased after hydration[b] (%)	WVP coefficient[c] × 10^4 (mg h^{-1} mm^{-1} $mmHg^{-1}$)	ACT permeability in 0.1 M HCl[d]		
					Lag time (min)	$P \times 10^5$ (cm s^{-1})	$D \times 10^8$ (cm^2 s^{-1})
GSA	32.9 ± 6.4	79.1 ± 17.5	140.4	1.73 ± 0.10	0.49 ± 0.09	7.96 ± 1.10	36.8 ± 7.8
MSA	38.7 ± 9.6	82.1 ± 24.3	112.1	2.22 ± 0.10	0.39 ± 0.07	15.8 ± 3.90	48.8 ± 8.5
GSA–MAS	61.6 ± 4.0	113.7 ± 6.6	84.6	1.47 ± 0.27	3.09 ± 0.45	2.70 ± 0.18	11.8 ± 1.2
MSA–MAS	60.5 ± 4.1	135.3 ± 2.5	123.6	1.67 ± 0.18	1.63 ± 0.27	5.06 ± 0.46	31.7 ± 5.5

[a] Data are the mean ± S.D., $n = 12$.
[b] ((Mean wet thickness − mean dry thickness)/mean dry thickness) × 100.
[c] Data are the mean ± S.D., $n = 4$.
[d] Data are the mean ± S.D., $n = 3$.

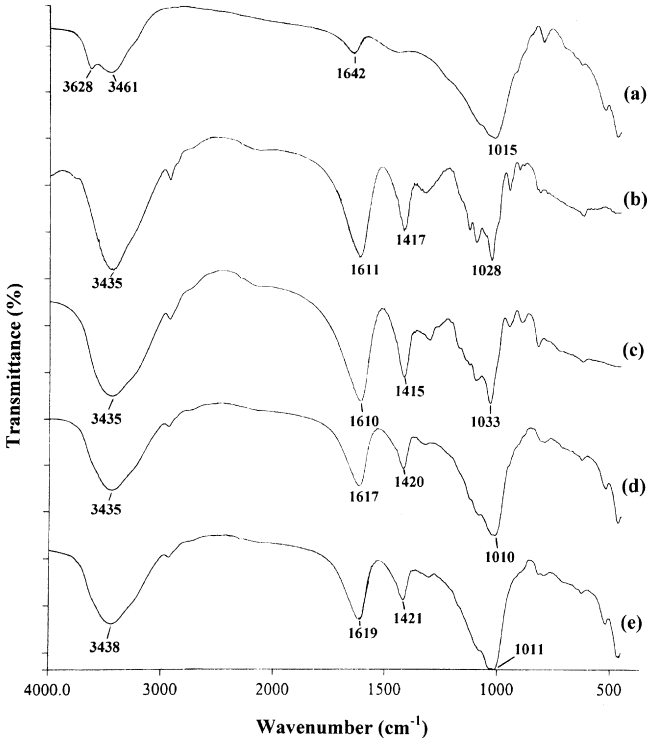

Fig. 3. FTIR spectra of MAS powder (a), GSA film (b), MSA film (c), GSA–MAS film (d) and MSA–MAS film (e).

peak of the silanol group (SiOH) at 3628 cm^{-1} disappeared in the spectra of SA–MAS films. These results could be expected if intermolecular hydrogen bonding could be created between the silanol groups on the surface of MAS and the hydroxyl or carboxyl groups of SA; the silanol groups had hydrogen bonding potential with some substances (Gupta et al., 2003). Furthermore, new evidence in this study, the lower wavenumber shift of the Si–O–Si stretching peak of MAS (from 1015 to 1010 cm^{-1}), could confirm the occurrence of intermolecular hydrogen bonding between SA and MAS. These findings indicated that GSA and MSA could similarly interact with MAS in both dispersions and films.

3.2. Appearance and thickness of films

Transparent SA films were obtained, whereas incorporation of MAS into the films gave opaque composite films. The thickness of the films is shown in Table 2. The dry thicknesses of GSA and MSA films were comparable. The GSA and MSA films gave significantly lower dry thicknesses than the GSA–MAS and MSA–MAS films because of the increase in the solid content in the films after incorporating MAS. The wet thickness of the films was remarkably greater than that of the dry films, indicating that the films could swell in an acidic medium. The MSA–MAS films showed higher percentages of thickness after hydration than the GSA–MAS films. This suggested that incorporating MAS into the GSA films could reduce the swelling properties in an acidic medium, which may affect the water uptake and drug permeability of the films.

3.3. DSC and PXRD studies

DSC curves of the films are presented in Fig. 4. The MSA powder presented a lower temperature and sharpness of the exothermic decomposition peak than the GSA powder (Fig. 4b and e). The MSA and GSA films had exothermic peaks at about 212.4 and 217.9 °C (Fig. 4c and f), respectively, which followed with an endothermic peak. This may be due to a recrystallization and a phase transition of SA after heat induction. These peaks shifted to lower temperatures when MAS was incorporated into the films (Fig. 4d and g), which was similar to the results of a previous study (Pongjanyakul et al., 2005b). This suggested that interaction of MAS and SA led to a change in the crystal structure formed, where recrystallization of SA–MAS composites and their phase transition occurred at a lower temperature. Moreover, the composite films' exothermic peak was shifted to a higher temperature and the intensity of the peak was reduced. This indicated that incorporation of MAS into the MSA and GSA films caused a similar change of thermal behavior.

The crystallinity of the films was investigated using powder X-ray diffractometry. The MAS powder showed an outstanding diffraction peak at 7.1° (2θ) (Fig. 5a), indicating the basal spacing of MAS, which represented 1.22 nm of the silicate layer thickness of MAS (Darder et al., 2003). A broad diffraction peak at 14° (2θ) was observed in the GSA and MSA films (Fig. 5b and c), respectively. The GSA–MAS and MSA–MAS films showed stronger intensity peaks at the same position as the basal spacing peak of MAS (Fig. 5d and e). This indicated that SA was unable to intercalate between the

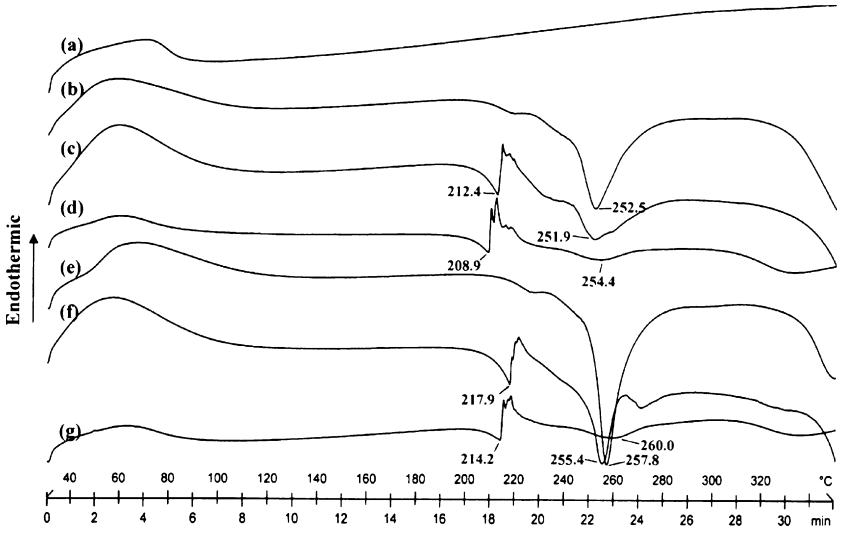

Fig. 4. DSC thermograms of MAS powder (a), MSA powder (b), MSA film (c), MSA–MAS film (d), GSA powder (e), GSA film (f) and GSA–MAS film (g).

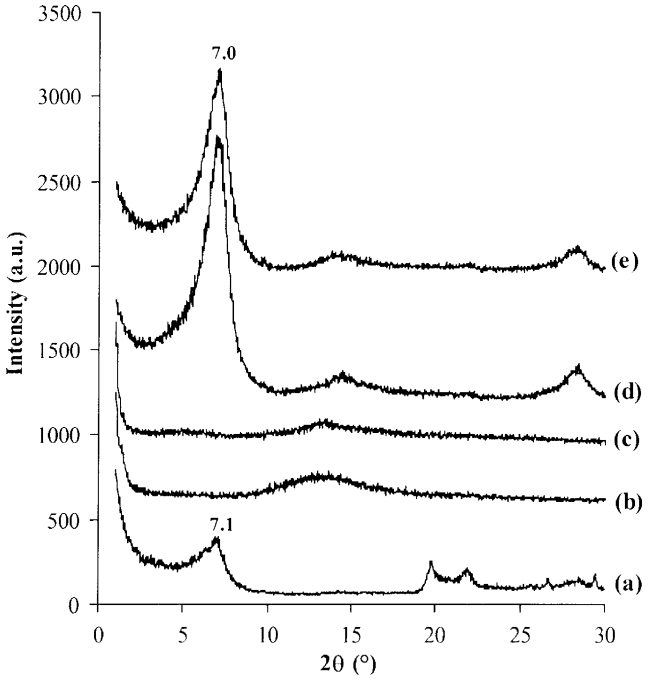

Fig. 5. PXRD patterns of MAS powder (a), and GSA (b), MSA (c), GSA–MAS (d) and MSA–MAS films.

silicate layers, but higher crystallinity of the films resulted from a reaggregation of MAS silicate layers during the drying process, in which the flocculation of MAS in the SA dispersions (Fig. 2b and c) may have led to the reaggregation process of MAS. However, it was observed that a stronger intensity peak at 7° (2θ) was found in the GSA–MAS films compared with that of the MSA–MAS films. This may be due to higher crystallinity of the GSA–MAS films, suggesting that a higher density of the ordered structure of the GSA and MAS was formed (Peppas, 1987).

3.4. Water uptake and erosion of the films

The percent water uptake and erosion of the films in 0.1 M HCl is shown in Fig. 6. The GSA films had lower water uptake percentages than the MSA films, whereas no differences in the erosion of both films were found. The water uptake and erosion of the films remarkably decreased when MAS was added. The water uptake of the GSA–MAS films was lower than that of the MSA–MAS films, and similar erosion was observed. In an acidic medium, SA was rapidly changed to water-insoluble alginic acid (Østberg et al., 1994), so the intact films were visually observed. The erosion of the films occurred rapidly (within 5 min) (Pongjanyakul and Puttipipatkhachorn, 2007) because of dissolution of some SA on the surface of the films. Alginic acid in the hydrated films had weaker intermolecular bonding (Aslani and Kennedy, 1996). This led to a large aqueous pore in the films and high water uptake was obtained. However, the considerably lower water uptake of the GSA films was observed because GSA had a stronger gel in acidic medium compared to MSA (Draget et al., 1994). This suggested that the GSA films possessed smaller aqueous pore channels and denser matrix structures than the MSA films. Incorporation of MAS could reduce the water uptake of the SA films, suggesting that the interaction of SA and MAS gave a denser matrix structure of the films. Moreover, the GSA–MAS films presented smaller aqueous pore channels than the MSA–MAS films. This could possibly explain that the higher crystallinity of the GSA–MAS films may reduce the water uptake capacity in acidic medium when compared with the MSA–MAS films.

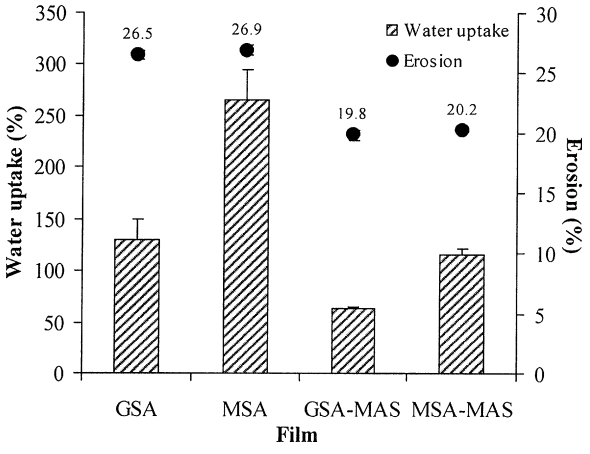

Fig. 6. Water uptake and erosion of SA and SA–MAS films in 0.1N HCl. Each value is the mean ± S.D., $n = 4$.

3.5. Permeability of the films

The water vapor permeability of the SA and the SA–MAS films is presented in Table 2. The WVP coefficient of the GSA films was lower than that of the MSA films. This result was in agreement with the finding of Russo et al. (2007), in which GSA promoted the chain-to-chain interaction in the films. This led to a denser matrix structure similar to that of the GSA films. The decrease of the WVP coefficient was found in both films when adding MAS. However, the lower WVP coefficient, compared with the MSA–MAS films, was still obtained with the GSA–MAS films. This indicated that interactions between SA and MAS caused a denser matrix structure preventing permeation of small molecules such as water vapor.

Comparative ACT permeation profiles of the SA and the SA–MAS films in 0.1 M HCl showed a straight line (R^2 higher than 0.99) with a lag time, indicating that the ACT permeation reached a steady state and could be described using Fick's first law. The ACT permeation parameters are listed in Table 2. The lag time of the ACT permeation across the GSA films seemed longer than that of the MSA films, whereas the P value of the GSA films was obviously lower than that of the MSA films. It was indicated that the GSA films had lower permeability in an acidic medium than the MSA films. The D values calculated using Eq. (7), using the wet thickness in Table 2, showed that the GSA films also gave lower D values than the MSA films. This is likely due to lower water uptake of the GSA films, producing smaller aqueous pore channels for ACT diffusion. The effect of MAS on ACT permeability of the SA films was also presented in Table 2. Incorporation of MAS into the SA films caused an increase in the lag time and a decrease in P and D values when compared with the SA films. However, the GSA–MAS films still provided lower P and D values than the MSA–MAS films. This suggested that interaction between SA and MAS brought about smaller aqueous pore channels and higher tortuosity of pore channels of the SA films.

The permeability of the GSA–MAS and MSA–MAS films using non-electrolyte and amine compounds was investigated in this study. In the case of parabens, the donor compartments of the diffusion cells were contained using paraben suspensions with saturated solutions. The solubility of MP, PP, and BP was found to be 4.10 ± 0.03, 0.57 ± 0.02, and 0.34 ± 0.02 mg/ml ($n = 3$), respectively. The permeation parameters of non-electrolyte and amine compounds are summarized in Fig. 7. As expected, the GSA–MAS films gave longer lag times and lower P and D values of all compounds than the MSA–MAS films, the reasons for which were discussed

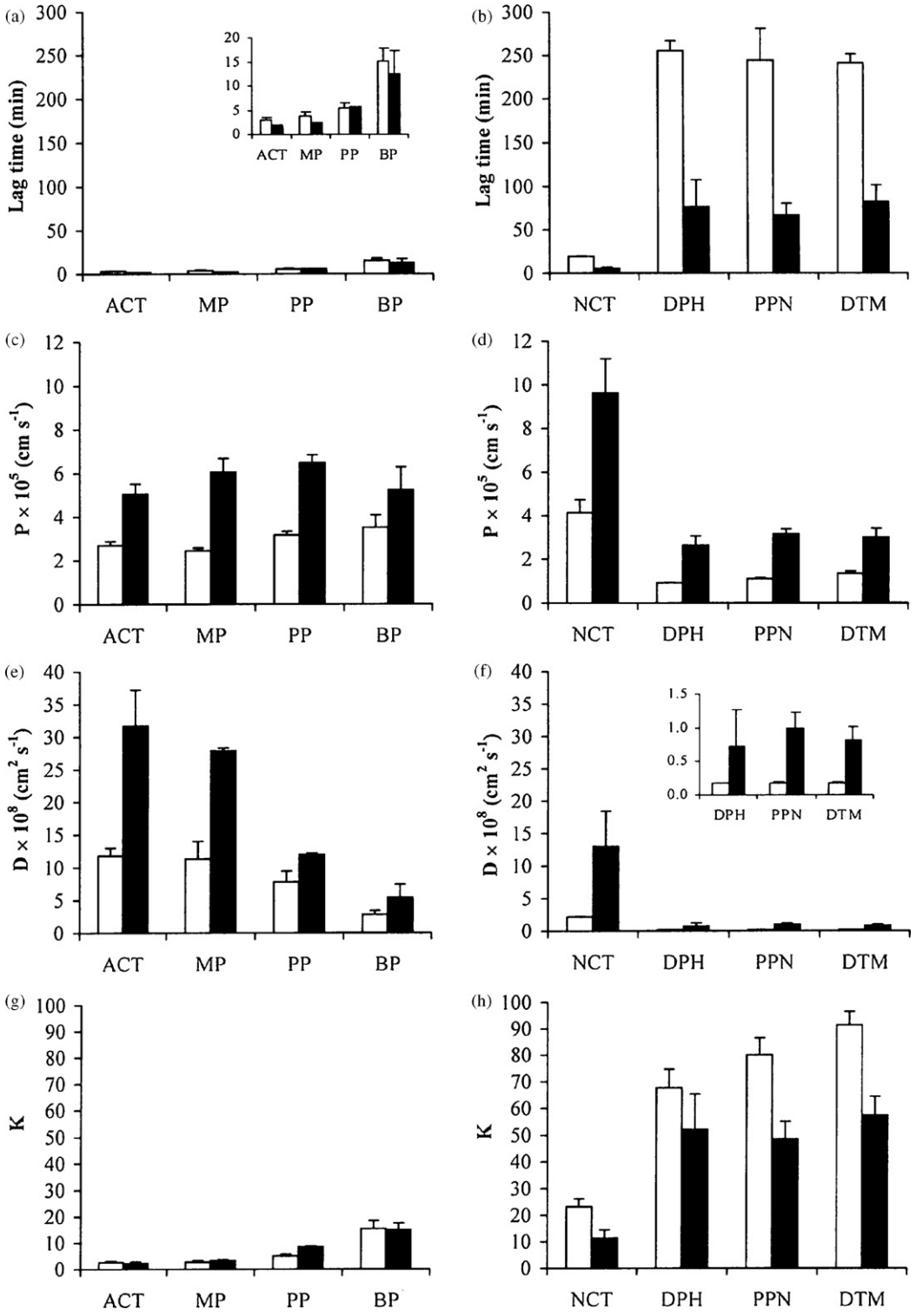

Fig. 7. Lag time (a and b), permeability coefficient (c and d), diffusion coefficient (e and f), and partition coefficient (g and h) of non-electrolyte and amine compounds when using GSA–MAS (open bars) and MSA–MAS (closed bars) films. Each value is the mean ± S.D., $n = 3$.

previously. A longer lag time was observed in non-electrolyte and amine compounds when the molecular weight of the compounds increased. Moreover, the lag times of the amine compounds were remarkably longer than those of neutral compounds. This was due to an adsorption of positively charged amine compounds onto the negatively charged sites of the MAS silicate layers (Sánchez-Matrin et al., 1981; Suksri and Pongjanyakul, 2008). The *P* values of the non-electrolyte compounds were quite similar, indicating that the molecular weight did not affect the *P* value. However, NCT gave higher *P* values than the other amine compounds. The *D* values of the non-electrolyte compounds decreased with increasing molecular weight, and similar results were obtained using the amine compounds. In contrast, greater *K* values were found with increasing molecular weight. It was observed that the type of amine group

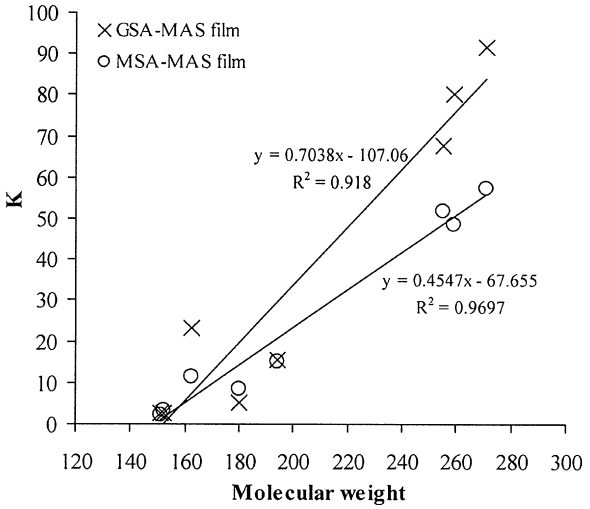

Fig. 8. Relationship between molecular weight and *K* values of non-electrolyte and amine compounds across GSA–MAS and MSA–MAS films.

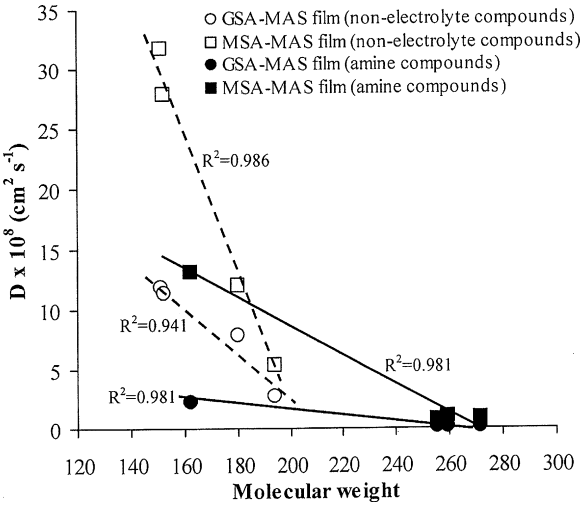

Fig. 9. Relationship between molecular weight and *D* values of non-electrolyte (open symbols) and amine (closed symbols) compounds across GSA–MAS and MSA–MAS films. The broken and solid lines are the regression lines of non-electrolyte and amine compounds, respectively.

in the molecular structure, such as a secondary amine group of DPH and PPN, and a tertiary amine group of DTM, did not affect the permeability of the composite films. Moreover, the permeation parameters of DPH and PPN, which had a side chain in the structure, were no different than those of DTM that were composed of a four-ringed structure. However, the fastest permeation value was found with NCT; even through it contained two amine group, it had the lowest molecular weight.

The relationship between the molecular weight of permeants and the permeation parameters was also investigated. The molecular weight of permeants showed a poor relationship with the *P* values (R^2 less than 0.62, data not shown). However, a good linearity between the molecular weight and the *K* values was obtained, with an R^2 value of more than 0.92 and 0.97 for the GSA–MAS and MSA–MAS films, respectively (Fig. 8). Moreover, the slope of the relationship with GSA–MAS was higher than that of the MSA–MAS films. This result suggested that the higher molecular weight of the permeants had stronger affinity with MAS in the composite films, particularly the amine compounds which possessed a positive charge in acidic medium. The smaller aqueous pore and higher tortuosity of microchannels of the GSA–MAS films caused an increase in the adsorption of permeants by MAS silicate layers that dispersed in the films. This resulted in the higher *K* values of the GSA–MAS films. Furthermore, the molecular weight of all permeants could be described by an exponential function with the *D* values in both composite films (Fig. 9). In most polymeric membranes, it is possible to relate log *D* with log MW for a linear function (Flynn et al., 1974); the results of this study showed linearity between log *D* and log MW, with R^2 higher than 0.90 and 0.98 for the GSA–MAS and MSA–MAS films, respectively. However, an alternative approach was found, showing that a good linearity between the relationship of the *D* values and MW could be directly found in each type of compound (Fig. 9). It can be seen that the increasing molecular weight of permeants provided slower diffusion mobilities in aqueous pore channels; this could be observed in the case of parabens, where the diffusivity decreased with an increasing number of hydrocarbon side chains (Flynn et al., 1974).

Two mechanisms of diffusive transport of permeants in a polymeric film had been previously purposed (Thacharodi and Panduranga Rao, 1993). The first is the partition mechanism of permeants into polymeric films, and the diffusion process in the polymer fraction progressed across the films. Permeability is mainly determined by the solubility of the permeant in the polymer. The other mechanism was pore mechanism. The permeant was presumed to diffuse across microchannels within the structure of hydrated films. The diffusion process was related to molecular weight and solubility of the permeants. In this study, it is likely that both mechanisms could be used to explain the diffusion of the compounds through the SA–MAS films. The microchannels of the SA–MAS films in the acidic medium could be formed because of the water uptake and swelling properties of the composite films. The non-electrolyte compounds with low *K* values may mainly diffuse through the composite films using microchannels. In contrast, the strong affinity of the amine compounds to the MAS in the composite films, which caused high *K* values, may be described using both mechanisms. The partition mechanism probably predominated in the initial stage of the diffusion process, which could be observed from a long lag time. Then, the diffusion of the compounds progressed across the composite films via diffusion in the route of the microchannels; this process depended on the molecular weight of the compounds.

4. Conclusion

The GSA and MSA had similar interactions with MAS in both dispersions and films. However, the crystallinity of the GSA–MAS films was possibly higher than that of the MSA–MAS films. This presented a higher density of matrix structure of the GSA–MAS composite, resulting in lower water uptake in an acidic medium. Consequently, the drug permeability of the GSA–MAS films was obviously lower than that of the MSA–MAS films. The permeation parameters, such as diffusion and partition coefficients, were directly related to the molecular weight of the non-electrolyte and amine compounds. This study suggested that the transport of the non-electrolyte compounds across the SA–MAS films was predominantly controlled by diffusion process in aqueous-filled microchannels, whereas both partition and pore mechanisms occurred concurrently for the transport of the amine compounds. These findings also suggest that the SA–MAS films could offer potential in the development for modulating drug release from coated tablets, which is dependent on the molecular weight of drug in the tablets and the ratio of the block structure of SA used in the films.

Acknowledgments

The author wishes to thank the Commission on Higher Education, the Ministry of Education (Bangkok, Thailand) and the Thailand Research Fund (Bangkok, Thailand) for financial support (Grant no. RMU4980022). The author also thanks the Faculty of Pharmaceutical Sciences and the Center for Research and Development of Herbal Health Products, Khon Kaen University (Khon Kaen, Thailand) for technical support.

References

Alexandre, M., Dubois, P., 2000. Polymer-layered silicate nanocomposites: preparation, properties and uses of a new class of materials. Mater. Sci. Eng. 28, 1–63.

Aslani, P., Kennedy, R.A., 1996. Studies on diffusion in alginate gels. I. Effect of cross-linking with calcium or zinc ions on diffusion of acetaminophen. J. Control. Release 42, 75–82.

Ciullo, P.A., 1981. Rheological properties of magnesium aluminum silicate/xanthan gum dispersions. J. Soc. Cosmet. Chem. 32, 275–285.

Ciullo, P.A., Braun, D.B., 1991. Clay/carbomer mixtures enhance emulsion stability. Cosmet. Toilet. 106, 89–95.

Darder, M., Colilla, M., Ruiz-Hitzky, E., 2003. Biopolymer-clay nanocomposites based on chitosan intercalated in montmorillonite. Chem. Mater. 15, 3774–3780.

Draget, K.I., 2000. Alginates. In: Philips, G.O., Williams, P.A. (Eds.), Handbook of Hydrocolloids. Woodhead Publishing, Cambridge, pp. 379–395.

Draget, K.I., Skjåk Bræk, G., Smidsrød, O., 1994. Alginic acid gels: the effect of alginate chemical composition and molecular weight. Carbohydr. Polym. 25, 31–38.

Flynn, G.L., Yalkowsky, S.H., Roseman, T.J., 1974. Mass transport phenomena and models: theoretical concepts. J. Pharm. Sci. 63, 479–510.

Gupta, M.K., Vanwert, A., Bogner, R.H., 2003. Formation of physical stable amorphous drugs by milling with Neusilin. J. Pharm. Sci. 92, 536–551.

Julian, T.N., Radebaugh, G.W., Wisniewski, S.J., 1988. Permeability characteristics of calcium alginate films. J. Control. Release 8, 165–169.

Katti, K.S., Sikdar, D., Katti, D.R., Ghosh, P., Verma, D., 2006. Molecular interaction in intercalated organically modified clay and clay–polycaprolactam nanocomposites: experiments and modeling. Polymer 47, 403–414.

Kibbe, H.A., 2000. Handbook of Pharmaceutical Excipients, 3rd edition. American Pharmaceutical Association, Washington, pp. 295–298.

Kohn, R., 1975. Ion binding on polyuronates: alginate and pectin. Pure Appl. Chem. 42, 371–397.

Lemoine, D., Wauters, F., Bouchend'homme, S., Préat, V., 1998. Preparation and characterization of alginate microspheres containing a model antigen. Int. J. Pharm. 176, 9–19.

Limmatvapirat, S., Limmatvapirat, C., Luangtana-anan, M., Nuntanid, J., Oguchi, T., Tozuka, Y., Yamamoto, K., Puttipipatkhachorn, S., 2004. Modification of physicochemical and mechanical properties of shellac by partial hydrolysis. Int. J. Pharm. 278, 41–49.

Martin, A., 1993. Physical Pharmacy, 4th edition. Lea&Febiger, Philadelphia, pp. 324–361, 453–476.

Østberg, T., Lund, E.M., Graffner, C., 1994. Calcium alginate matrices for oral multiple unit administration. IV. Release characteristics in different media. Int. J. Pharm. 112, 241–248.

Peppas, N.A., 1987. Diffusion through polymer. In: Kydonieus, A.F., Berner, B. (Eds.), Transdermal Delivery of Drugs, vol. 1. CRC Press, Boca Raton, pp. 17–28.

Pongjanyakul, T., Priprem, A., Puttipipatkhachorn, S., 2005a. Influence of magnesium aluminium silicate on rheological, release and permeation characteristics of diclofenac sodium aqueous gels in-vitro. J. Pharm. Pharmacol. 57, 429–434.

Pongjanyakul, T., Priprem, A., Puttipipatkhachorn, S., 2005b. Investigation of novel alginate–magnesium aluminum silicate microcomposite films for modified-release tablets. J. Control. Release 107, 343–356.

Pongjanyakul, T., Puttipipatkhachorn, S., 2007. Alginate–magnesium aluminum silicate films: effect of plasticizers on film properties, drug permeation and drug release from coated tablets. Int. J. Pharm. 333, 34–44.

Porter, S.C., Ridgway, K., 1982. The permeability of enteric coatings and the dissolution rates of coated tablets. J. Pharm. Pharmacol. 34, 5–8.

Remuñán-López, C., Bodmeier, R., 1997. Mechanical, water uptake and permeability properties of crosslinked chitosan glutamate and alginate films. J. Control. Release 44, 215–225.

Russo, R., Malinconico, M., Santagata, G., 2007. Effect of cross-linking with calcium ions on the physical properties of alginate films. Biomacromolecules 8, 3193–3197.

Sánchez-Matrin, M.J., Sánchez-Camazano, M., Vicente-Hernández, M.T., Dominguez-Gil, A., 1981. Interaction of propranolol hydrochloride with montmorillonite. J. Pharm. Pharmacol. 33, 408–410.

Sriamornsak, P., Kennedy, R.A., 2008. Swelling and diffusion studies of calcium polysaccharide gels intended for film coating. Int. J. Pharm. 358, 205–213.

Suksri, H., Pongjanyakul, T., 2008. Interaction of nicotine with magnesium aluminum silicate at different pHs: Characterization of flocculate size, zeta potential and nicotine adsorption behavior. Colloids Surf. B 65, 54–60.

Thacharodi, D., Panduranga Rao, K., 1993. Release of nifedipine through crosslinked chitosan membranes. Int. J. Pharm. 96, 33–39.

Tuovinen, L., Peltonen, S., Järvinen, K., 2003. Drug release from starch-acetate films. J. Control. Release 91, 345–354.

Zatz, J.L., Kushla, G.P., 1989. Gels. In: Lieberman, H.A., Rieger, M.M., Banker, G.S. (Eds.), Pharmaceutical Dosage Forms: Disperse Systems, vol. 19. Marcel Dekker, New York and Basel, pp. 495–510.